Monitoring of 3D large surface deformation in coal mines through the integration of synthetic aperture radar pixel offset tracking and probability integration function model

Bingqian Chen[1, 2,*], Da Jiang[3], Jian Zhang[3], Jian Gao[1], Xueting Fan[4]

1. School of Geography, Geomatics and Urban-Rural Planning, Jiangsu Normal University, Xuzhou 221116, China

2. Hunan Province Key Laboratory of Coal Resources Clean-utilization and Mine Environment Protection, Xiangtan 411201, China

3. Henan Surveying and Mapping Engineering Institute, Zhengzhou 450046, China

4. Provincial Geomatics Centre of Jiangsu, Nanjing 210013, China

bqccumt@gmail.com

ABSTRACT. *Considering the severity of surface deformation in coal mines and the limitation of the popular deformation monitoring technique interferometric synthetic aperture radar (InSAR), this paper attempts to measure the large deformation caused by coal mining and disclose the ground deformation law in an all-round way. For this purpose, the pixel offset tracking (POT) was integrated with the probability integration function model (PIFM) to track the 3D large deformation of the surface based on SAR image amplitude information. Firstly, the line of sight (LOS) deformation was acquired by the POT, while the vertical, east-west and south-north deformations were estimated by the PIFM based on the LOS deformation. After that, the proposed method was applied to monitor the surface deformation of Daliuta mine lot in China's Shaanxi Province, and the results on 3D large deformation were compared against those obtained by the GPS station. It is found that the root means square error (RMSE) was 16.5 cm in the vertical direction, 12.2cm in the east-west horizontal direction, and 13.4m in the north-south horizontal direction, indicating the proposed method is accurate and reliable. The research findings shed new light on hazard monitoring in coal mines.*

RÉSUMÉ. *Compte tenu de la gravité des déformations superficielles dans les mines de charbon et de la limitation du radar à synthèse d'ouverture interférométrique (InSAR), technique de surveillance de la déformation très répandue, cet article tente de mesurer la déformation*

importante provoquée par l'extraction du charbon et de révéler la loi de déformation du sol de manière globale. À cette fin, le suivi de décalage de pixel (POT) a été intégré au modèle de fonction d'intégration de probabilité (PIFM) afin de suivre la grande déformation 3D de la surface sur la base des informations d'amplitude de l'image SAR. Premièrement, la déformation de la ligne de visée (LOS) a été obtenue par le biais du POT, tandis que les déformations verticales, est-ouest et sud-nord ont été estimées par le PIFM sur la base de la déformation LOS. Après cela, la méthode proposée a été appliquée pour surveiller la déformation de surface du lot minier de Daliuta dans la province du Shaanxi de la Chine, et les résultats concernant les grandes déformations 3D ont été comparés à ceux obtenus par la station GPS. Il a été constaté que l'erreur quadratique moyenne (RMSE) était de 16,5 cm dans la direction verticale, de 12,2 cm dans la direction horizontale est-ouest et de 13,4 m dans la direction horizontale nord-sud, indiquant que la méthode proposée est précise et fiable. Les résultats de la recherche offrent une nouvelle perspective pour la surveillance des dangers dans les mines de charbon.

KEYWORDS: *interferometric synthetic aperture radar (InSAR), large deformation, deformation monitoring, pixel offset tracking (POT), probability integration function model (PIFM).*

MOTS-CLÉS: *radar à synthèse d'ouverture interférométrique (InSAR), déformation importante, surveillance de la déformation, suivi de décalage de pixel (POT), modèle de fonction d'intégration de probabilité (PIFM).*

DOI:10.3166/I2M.17.507-519

1. Introduction

Surface deformation and other damages are commonplace in coal mines. Traditionally, the mining deformation is monitored by triangulation, levelling and GPS survey. However, these methods often cannot output complete monitoring information, despite their high cost and heavy workload (Song *et al.*, 2012; Li *et al.*, 2011; Wang *et al.*, 2008; Wang *et al.*, 2011).

The interferometric synthetic aperture radar (InSAR), an innovative approach for ground subsidence monitoring, can capture the subtle displacement of surface resolution elements in the millimeter scale (Massonnet *et al.*, 1993). Thanks to its fast speed, high precision, large coverage and other advantages, the InSAR has been extensively adopted for the monitoring of surface deformation in coal mines (Yang *et al.*, 2010; Fan *et al.*, 2011; Chen *et al.*, 2013; Fan *et al.*, 2014; Li *et al.*, 2015; Abdikan *et al.*, 2014; Greif and Vlcko, 2011; Bateson *et al.*, 2015).

Nevertheless, the surface deformation in coal mines is sometimes too fast and steep to be detected by InSAR interferometry. In this case, the deformation phase cannot be restored correctly if it is directly unwrapped. To improve the deformation detection gradient of InSAR, Reference puts forward the interpolation multi-view method while Reference (Zhao *et al.*, 2014) adopts the full resolution method for single interferogram. However, neither method manage to fundamentally eliminate the large deformation (e.g. meter scale deformation) in the mining area. Besides the measurement of interferometric phase, the SAR image amplitude information is also a research hotspot in deformation estimation.

Based on SAR image amplitude information, the pixel offset tracking (POT) has been successfully applied for information monitoring in such places as glaciers, volcanoes, and landslide areas (Strozzi *et al.*, 2002; Fielding *et al.*, 2013; Manconi *et al.*, 2014). Reference (Zhao *et al.*, 2013) is the first to implement the POT to monitor the surface deformation in mining areas, and realizes the monitoring accuracy of 1/25 pixel. Reference (Huang *et al.*, 2016) adopts the POT to observe the deformation in Daliuta mine lot, Shaanxi province, China, and puts the maximum line-of-sight (LOS) deformation quantity at 3.6m. Nevertheless, the existing studies on POT application in coal mines only concentrate on the 1D vertical deformation field, failing to consider the effect of horizontal deformation. Actually, the underground mining may cause both vertical and horizontal deformations. Thus, the results from 1D vertical direction cannot fully reflect the true deformation state in the mine lot and may lead to misjudgment.

In light of the above, this paper attempts to measure the large deformation caused by coal mining and disclose the ground deformation law in an all-round way. For this purpose, the POT was integrated with the probability integration function model (PIFM) to track the 3D large deformation of the surface. By the integrated method, the LOS deformation was acquired by the POT, while the vertical, east-west and south-north deformations were estimated by the PIFM based on the LOS deformation. After that, the proposed method was applied to monitor the surface deformation of Daliuta mine lot in China's Shaanxi Province, and the results on 3D large deformation were compared against those obtained by the GPS station, aiming to verify the accuracy and reliability of our method.

The remainder of this paper is organized as follows: Section 2 introduces the integrated method, as well as the algorithms in each step; Section 3 presents the datasets for our experiment and reports the experimental results; Section 4 discusses the experimental results and draws the conclusions.

2. Method

2.1. Acquisition of POT-based LOS deformation

The core of POT technology is the cross-correlation algorithm, just like a similarity measure in the image match process. Assume that there are a reference image I_1 and a secondary image I_2, as shown in Fig. 1, $f(x, y)$ is the amplitude value of the reference block; $t(x-u, y-v)$ is the amplitude value of the search block. In order to search the block that responds to $f(x, y)$ in the auxiliary image, the correlation coefficient ρ is imported to represent the correlation between two blocks, and its value may fall within (-1, 1), when taking value -1, it means that the two blocks have an equivalent amplitude but are inverted in the directions; the value 0 shows that there is no correlation between the two blocks, and the value 1 means that the amplitude values of the two blocks coincides, so that they correlate to each other to a maximum extent. The correlation coefficient ρ is calculated as follows:

$$\rho(\mathbf{x},\mathbf{y}) = \frac{\sum_{\mathbf{x},\mathbf{y}}(f(x,y)-\overline{f})(t(x-u,y-v)-\overline{t})}{\left(\sum_{\mathbf{x},\mathbf{y}}(f(x,y)-\overline{f})^2\sum_{\mathbf{x},\mathbf{y}}(t(x-u,y-v)-\overline{t})^2\right)^{1/2}} \quad (1)$$

Assume that the pixel point (x_0, y_0) is most highly correlated in the search process, it is regarded that the matching point matches the reference block center pixel point (x, y), and the coordinate difference between the two corresponds to the offset along the range direction and Azimuth. In order to improve the accuracy of the match point position, the main and auxiliary images are often oversampled at a factor selected in this way that the combined effects from image resolution and computational efficiency should be concerned.

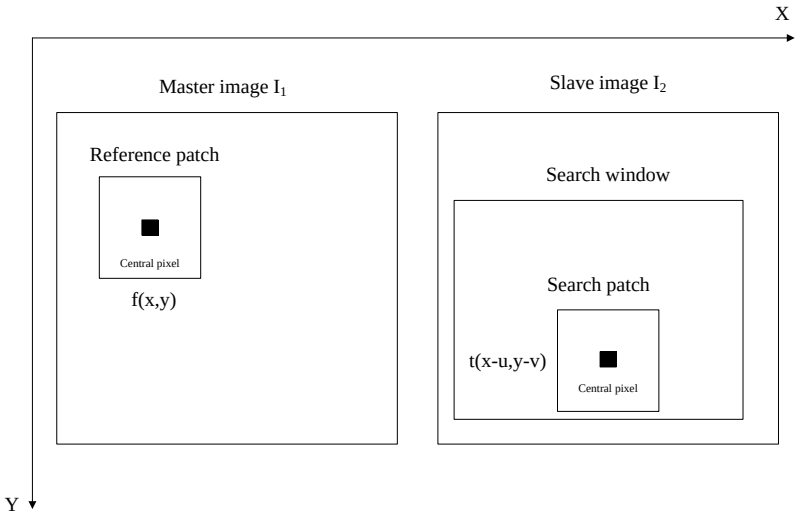

Figure 1. Schematic diagram of cross correlation algorithm

The offset obtained by using the cross-correlation algorithm is subjected to factors such as satellite orbit position difference, topographic relief, surface deformation and ionized stratum. Ignored the effects from the topography and the ionized stratum, the offset at this time can be considered as a composition of the offsets caused by the satellite orbit position difference and by surface deformation:

$$O_{\text{reg}} = O_{\text{orb}} + O_{\text{def}} \quad (2)$$

Where O_{reg} represents the total offset obtained by the cross-correlation algorithm; O_{orb} represents the offset caused by the satellite orbit position difference; O_{def} represents the offset caused by the surface deformation. In order to extract the deformation displacement from the offset, the offset O_{orb} must be estimated and

subtracted from the O_{reg}. Take the mining subsidence as an example, except for the severe deformation of the surface right above the mining face, less deformation occurs in the other areas. The earth's surface far away from the working surface basically has no deformation, which can be regarded as a stable area. The offset of the pixels in these areas can be considered approximately equals to that caused by orbit. With these offsets and their respective pixel coordinates, a biquadratic polynomial model can be built:

$$O_{\text{orb}} = a_0 + a_1 x + a_2 y + a_3 xy + a_4 x^2 + a_5 y^2 \tag{3}$$

Where x and y represent the coordinates under the radar coordinate system, respectively, a_0, a_1, a_2, a_3, a_4 and a_5 are the polynomial coefficients to be solved, and several points (generally greater than 12) are selected in the stable area to solve the multinomial coefficient solution by the least squares criterion. The registration offset obtained by using the equation (3) can be used as an estimated value of O_{orb}. According to the estimated value, the surface deformation offset O_{def} can be available by subtracting the value from equation (2), including two components along the slant range and the azimuth direction. This paper only uses the slant range deformation filed.

2.2. Establishing the POT- and PIFM-based 3D deformation model

PIFM uses the normal distribution function as the influence function and the integral method to represent the surface deformation. Since the theoretical basis of the method is stochastic medium theory, it is also called the stochastic medium theory (Litwiniszyn, 1974). As shown in Fig. 2, the ground coordinate system xOy and the coal seam coordinate system sO_1t are taken. In the horizontal or near horizontal coal seam mining unit B (s, t), according to the principle of probability integral model, the subsidence value of arbitrary surface point A (x, y) is caused as follows:

$$W(x,y) = (1/r^2) \cdot \exp(-\pi \cdot ((x-s)^2 + (y-t)^2 / r^2)) \tag{4}$$

Correspondingly, the slopes $I_x(x,y)$ and $I_y(x,y)$, horizontal displacements $U_x(x,y)$and $U_y(x,y)$of the surface A (x,y) along x and y directions are given as follows:

$$I_x(x,y) = dW(x,y)/dx = (-2\pi / r^2) \cdot (x-s) \cdot W(x,y) \tag{5}$$

$$I_y(x,y) = dW(x,y)/dy = (-2\pi / r^2) \cdot (y-t) \cdot W(x,y) \tag{6}$$

$$\begin{aligned} U_x(x,y) &= (b \cdot H / \tan\beta) \cdot dW(x,y)/dx \\ &= (-2\pi \cdot b \cdot H) \cdot (x-s) / (r^2 \cdot \tan\beta) \cdot W(x,y) \end{aligned} \tag{7}$$

$$\begin{aligned} U_y(x,y) &= (b \cdot H / \tan\beta) \cdot dW(x,y)/dy \\ &= (-2\pi \cdot b \cdot H) \cdot (x-t) / (r^2 \cdot \tan\beta) \cdot W(x,y) \end{aligned} \tag{8}$$

In the above formula, b is the horizontal displacement coefficient; r is the major effect radius at the mining unit B; $r = H/\tan\beta$; H is the mining depth of the unit B; tanβ is the main effecting angle tangent; θ is the mining effect propagation angle. According to the equations (5) ~ (8), it can be seen that the horizontal displacement, $U_\phi(x, y)$, of any point (x, y) on the surface caused by horizontal or near horizontal coal seam mining in any direction (x, y) and the slope, $T_\phi(x, y)$, in the corresponding direction are proportional to each other:

$$U_\phi(x,y) = b \cdot H / \tan\beta \cdot I_\phi(x,y) \tag{9}$$

Assume that the surface subsidence of the mine area is $m \times n$, and $H(i, j)$, $W(i, j)$, $I_{EW}(i, j)$, $I_{NS}(i, j)$ (i = 1, 2,……,m; j = 1, 2,……,n) are the mining depth, the subsidence, slopes along east-west and north-south directions at the pixel (i, j). According to the definition of slopes in coal mine, it can be known that:

$$\begin{cases} I_{NS}(i,j) = [W(i+1,j) - W(i,j)]/\Delta y \\ I_{EW}(i,j) = [W(i,j+1) - W(i,j)]/\Delta x \end{cases} \tag{10}$$

According to equations (9)~(10), the horizontal displacements $U_{EW}(i, j)$, $U_{NS}(i, j)$ of the pixel (i, j) in the east-west and south-north directions can be expressed as:

$$\begin{cases} U_{NS}(i,j) = b \cdot H / \tan\beta \cdot [W(i+1,j) - W(i,j)] / \Delta y \\ U_{EW}(i,j) = b \cdot H / \tan\beta \cdot [W(i,j+1) - W(i,j)] / \Delta x \end{cases} \tag{11}$$

In the equations (10)~(11), i=1, 2,…, m-1; j=1, 2,…, n-1, Δx, Δy are the spatial resolutions of SAR deformation maps in the east-west and south-north directions. As shown in Equation (11), the horizontal displacements of the surface of the mine area in the east-west and north-south directions can be expressed as the adjacent subsidence values. According to the radar imaging principle, the LOS deformation is a combination of vertical surface displacement, east-west and north-south horizontal displacements, and can be expressed as (Fialko *et al.*, 2001):

$$\begin{aligned} LOS(i,j) = {} & W(i,j)\cos(\theta(i,j)) - \sin(\theta(i,j))[U_{NS}\cos(\alpha - 3\pi/2) \\ & + U_{EW}\sin(\alpha - 3\pi/2)] \end{aligned} \tag{12}$$

Where α is the radar flight azimuth; θ is the radar incident angle, and (11) is substituted into (12):

$$LOS(i,j) = [C1\ C2\ C3]\begin{bmatrix} W(i,j) \\ W(i+1,j) \\ W(i,j+1) \end{bmatrix} \tag{13}$$

Where (i=1, 2, ……, m-1; j=1, 2, …… n-1)

$$C_1 = \cos(\theta(i,j)) + (b \cdot H \cdot \sin(\theta(i,j))/\tan\beta) \cdot (\cos(\alpha - 3\pi/2)/\Delta y + \sin(\alpha - 3\pi/2)/\Delta x)$$

$$C_2 = -b \cdot H \cdot \sin(\theta(i,j)) \cdot \cos(\alpha - 3\pi/2)/(\Delta y \cdot \tan\beta)$$

$$C_3 = -b \cdot H \cdot \sin(\theta(i,j)) \cdot \sin(\alpha - 3\pi/2)/(\Delta x \cdot \tan\beta)$$

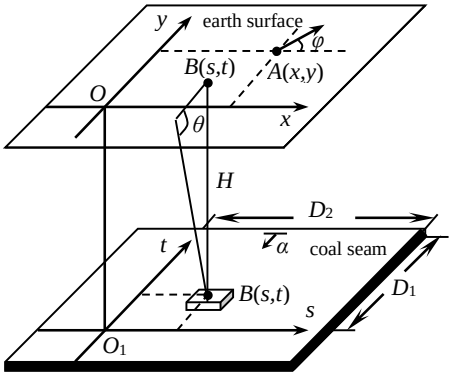

Figure 2. Spatial coordinate system for coal mining

In equation (13), there are (m−1)×(n−1) equations, and the unknowns is m×n. This is an underdetermined equation and its solution is not unique. In Literature, when PIM is used to solve the 3D deformation of the mine area, it is assumed that the contribution of the LOS shifting levelly of the basin edge is negligible and the back-substitution method is used to solve the equation. However, this method has no closure error check conditions. It is easy to cause error accumulation and affect the precision of the solution results. In order to avoid the error accumulation in the model, an iterative solution is used, as shown below:

(1) Assume that all pixels are not horizontally deformed, the vertical subsidence value of any point (i, j) is obtained by the equation (12), i.e. W(i, j)=LOS(i, j)/cos(θ(i, j));

(2) Equation (13) is used to solve the new LOS'(i, j), and the closure errors generate ΔLOS(i, j)= LOS'(i, j)- LOS(i, j) at this time;

(3) Assign the closure error ΔLOS(i, j), and generate a new LOS''(i, j), i.e. LOS''(i, j)= LOS(i, j)+ΔLOS(i, j);

(4) Repeat the steps (1)-(3) until the closure error ΔLOS(i, j) is less than a given threshold, the iteration ends up;

(5) The final w(i,j) obtained from the steps (1)-(4) is substituted into the equation (11) to solve the north-south and east-west horizontal displacements $U_{NS}(i, j)$ and $U_{EW}(i, j)$ of arbitrary pixels, finally achieving 3D deformation estimation of arbitrary pixels.

The key that the equations (11) and (13) are solved is to determine the parameters tanβ and *b*. In order to avoid the blindness of artificially selected model parameters and to realize the optimal selection of model parameters, this paper uses the genetic algorithm to intelligently obtain model parameters, refer to the Literature.

3. Experiment

3.1. Experimental area and data

The experimental area lies in the Daliuta mine area, Shaanxi Province, in west China. The full length of the working face in the study area is about 4547 m, the working face width is about 300 m, the average depth is 235 m, and the coal seam dip angle is 1°~3°. The coal mining operated from November 1, 2012 to March 25, 2013, and the mining direction marched from the southeast to the northwest directions. The location of the working face is shown in Fig. 3.

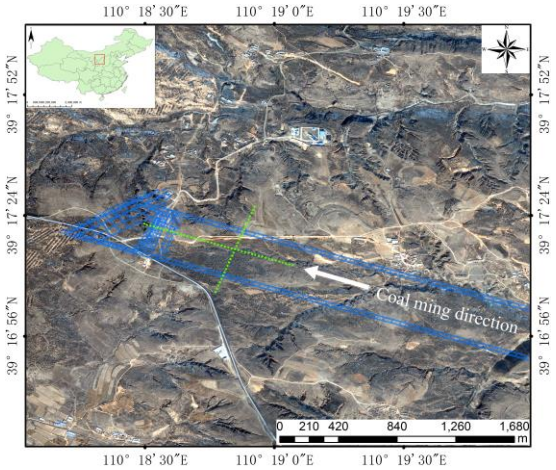

Figure 3. Layout of the observation station of the mining face

Table 1. TerraSAR-X satellite parameters

Master	Slave	Temporal baseline (days)	Perpendicular baseline (m)
2012/11/21	2013/04/02	132	-82.4

In this experiment, the SAR data in the High Resolution SpotLight mode of the TerraSAR-X satellite is used. The azimuth pixel spacing is 0.85 m; the distance pixel spacing is 0.91 m; the image is acquired on November 21, 2012 and on April 2, 2013. The detailed satellite parameters are shown in Table 1.

3.2. Acquisition of 3D deformation

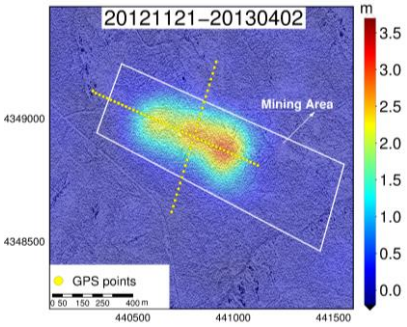

Figure 4. LOS direction deformation field, the positive value represents the movable deformation away from the satellite, and the negative value represents the movable deformation near the satellite

In order to obtain 3D deformation law of the surface of this area in extreme conditions, the method proposed in this paper is used to make an experimental study and analysis. To reduce the effects of terrain fluctuations, external SRTM elevation (DEM) data is used as an aid for registration with a resolution of 1"×1". Then, the LOS-oriented deformation field is obtained by carrying out the POT calculation on each set of SAR images. The search window size is set to 64×64 during the experiment, and the over-sampling factor is set to 2 in order to more accurately locate the maximum correlation value and the operation efficiency in the matching process. As shown in Fig. 4, the LOS direction deformation field is solved.

As shown in Fig. 4, the maximum deformation of LOS exceeds 3.5 m from November 21, 2012 to April 2, 2013, and the deformation trend coincides with the coal mining direction. The survey results reveal that the spread range and development trend of surface subsidence caused by coal mining can be acquired, but only one-dimensional LOS deformation results cannot fully reflect the surface deformation of the mine lot, and fall short of what's needed for the project.

Therefore, based on the LOS deformation field, a 3D deformation modelling is made with the method as described in 2.2. From the parameter file of TerraSAR-X satellite, the radar incident angle θ=42.43 degrees and the heading angle α =189.53 degrees can be obtained. In order to obtain the optimal model parameters, the model parameters are solved by the method in Section 2.3. During the experiment, the genetic algorithm population is set to 50, and the genetic algebra to 200 times, so that $tan\beta$ (tangent of the major influential angle) is finally available, up to 2.25, b(coefficient of horizontal displacement) is 0.26. Based on the above parameters and the obtained LOS deformation field, the vertical, north-south and east-west deformation fields are available, as shown in Fig. 5(a), (b) and (c), respectively.

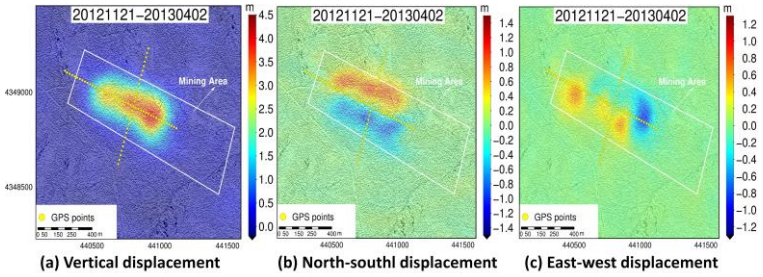

Figure 5. (a) Vertical deformation map, where the positive value represents surface subsidence; the negative value represents surface uplift; (b) North-south deformation, where the positive value represents the uphill direction of the mining area; the negative value represents the downhill direction of the mining area; (c) East-west deformation, where, the positive value represents the uphill direction of the mining area; the negative value represents the downhill direction of the mining area

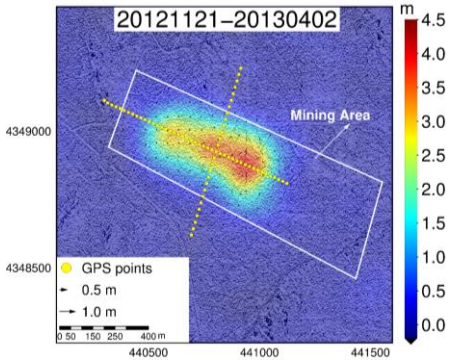

Figure 6. Layout of vertical subsidence and horizontal movement deformation, where the positive value represents surface subsidence, and the negative value represents surface uplift

As shown in Fig. 5(a), the vertical maximum deformation is about 4.4 m from November 21, 2012 to April 2, 2013, and the surface deformation has a tendency to get consistent with the coal mining direction, and the morphology in Fig. 5 (a) relatively approaches to that in Fig. 4, they all develop from a bowl shape to an approximately ellipsoidal one, while the subsiding basin has a higher subsidence value and gradually decreases toward the periphery.

As shown in Fig. 5(b), from November 21, 2012 to April 2, 2013, the maximum horizontal displacements in the north-south direction that points at distract raise and dip are basically equal, while the two horizontal displacement areas are more symmetrical. Its horizontal displacement values are about 1.4 m. Comparing Fig. 5(b), it can be seen from Fig. 5(c) that the maximum horizontal displacement in the east-west direction from November 21, 2012 to April 2, 2013 is about 1.2 m, and three horizontal displacement areas along the uphill direction of the mine and one along the downhill direction of the mining area appear. The deformations in the east-west and north-south directions are synthesized, as shown in Fig. 6. With the exploitation of working face, the horizontal displacement gradually extends up to 1 m, and points to goaf center. There is almost no horizontal displacement on the surface above the goaf center, and the horizontal displacement value above the mining boundary is the maximum and gradually decreases outward.

In order to test the accuracy of the experimental results, the 3D deformation results obtained by the experiment are compared to that from the GPS observation station in Fig. 3. The root mean square error of the vertical subsidence is 16.5 cm, and the maximum root mean square errors of maximum horizontal displacement in the east-west and the north-south directions are 12.2 cm and 13.4 cm, respectively, and the above accuracy can meet the needs of large deformation monitoring in coal mining areas.

4. Conclusions

Coal mining often causes severe ground deformation by a large gradient in a short time, which goes beyond the detectability scope of conventional InSAR technology. In order to trace the large deformation information of coal mining and discover the surface deformation law, this paper proposes a method that integrates the POT method based on SAR image amplitude information with PIFM. Take the working face of Daliuta mining area in Shaanxi Province, China as an example, based on the TerraSAR-X satellite data available from November 21, 2012 to April 2, 2013, the experiment conducted on the deformation monitoring using the method proposed in this paper exposes the deformation law of the 3D surface and the surface damage extent. The results show that the maximum deformation is about 4.4 m in vertical direction, and 1.2 m and 1.4 m in the east-west and north-south directions, respectively. The results from deformation monitoring are compared with the observations of the GPS: the root mean square error of vertical subsidence is 16.5 cm, and the root mean square errors of the horizontal displacement in the east-west and north-south directions are 12.2 cm and 13.4 cm, respectively, as required by the deformation monitoring project in the mine lots, so that this method has been

proven to be effective in the coal mining areas.

Acknowledgment

This work was funded by the Natural Science Foundation of China (No. 41702375), the Basic Research Project of Jiangsu Province (Natural Science Foundation, No. BK20160218) and Hunan Province Key Laboratory Foundation of Coal Resources Clean-utilization and Mine Environment Protection (No. E21801). The authors would also like to thank the German Aerospace Centre for providing the images (TerraSAR-X Science Plan, No. LAN1425 and LAN1173) over the study area. This work was also funded by the Jiangsu Provincial Bureau of Surveying Mapping and Geoinformation Research Project under Grant No. JSCHKY201803

REFERENCES

Abdikan S., Arikan M., Sanli F. B. (2014). Monitoring of coal mining subsidence in peri-urban area of Zonguldak city (NW Turkey) with persistent scatterer interferometry using ALOS-PALSAR. *Environmental Earth Sciences*, Vol. 71, No. 9, pp. 4081-4089. https://doi.org/10.1007/s12665-013-2793-1

Bateson L., Cigna F., Boon D., Sowter A. (2015). The application of the Intermittent SBAS (ISBAS) InSAR method to the South Wales Coalfield, UK. *International Journal of Applied Earth Observation and Geoinformation*, Vol. 34, No. 1, pp. 249-257. https://doi.org/10.1016/j.jag.2014.08.018

Chen B. Q., Deng K. Z., Fan H. D., Hao M. (2013). Monitoring large-scale deformation in mining area by D-InSAR and 3D laser scanning technology integration. *International Journal of Mining Science and Technology*, Vol. 23, No. 4, pp. 555-561. https://doi.org/10.1016/j.ijmst.2013.07.014

Fan H. D., Deng K. Z., Ju C. (2011). Land subsidence monitoring by D-InSAR technique. *Mining Science and Technology (China)*, Vol. 21, No. 6, pp. 869-872. https://doi.org/10.1016/j.mstc.2011.05.030

Fan H. D., Gu W., Qin Y., Xue J. Q., Chen B. Q. (2014). A model for extracting large deformation mining subsidence using D-InSAR technique and probability integral method. *Transactions of Nonferrous Metals Society of China*, Vol. 24, No. 4, pp. 1242-1247. https://doi.org/10.1016/S1003-6326(14)63185-X

Fialko Y., Simons M., Agnew D. (2001). The complete (3-D) surface displacement field in the epicentral area of the 1999 Mw7. 1 Hector Mine earthquake, California, from space geodetic observations. *Geophysical Research Letters*, Vol. 28, No. 16, pp. 3663-3066. https://doi.org/10.1029/2001GL013174

Fielding E. J., Lundgren P. R., Taymaz T., Yolsal-Çevikbilen S., Owen S. E. (2013). Fault-slip source models for the 2011 M 7.1 van earthquake in turkey from SAR interferometry, pixel offset tracking, GPS, and Seismic waveform analysis. *Seismological Research Letters*, Vol. 84, No. 4, pp. 579-593. https://doi.org/10.1785/0220120164

Greif V., Vlcko J. (2011). Monitoring of post-failure landslide deformation by the PS-InSAR technique at Lubietova in central Slovakia. *Environmental Earth Sciences*, Vol. 66, No. 6, pp. 1585-1595. https://doi.org/10.1007/s12665-011-0951-x

Huang J., Deng K., Fan H., Yan S. (2016). An improved pixel-tracking method for monitoring mining subsidence. *Remote Sensing Letters*, Vol. 7, No. 8, pp. 731-740. https://doi.org/10.1080/2150704X.2016.1183177

Li P. X., Tan Z. X., Yan L. L., Deng K. Z. (2011). Time series prediction of mining subsidence based on a SVM. *Mining Science and Technology (China)*, Vol. 21, No. 4, pp. 557-567. https://doi.org/10.1016/j.mstc.2011.02.025

Li Z. W., Yang Z. F., Zhu J. J., Hu J., Wang Y. J., Li P. X., Chen G. L. (2015). Retrieving three-dimensional displacement fields of mining areas from a single InSAR pair. *Journal of Geodesy*, Vol. 89, No. 1, pp. 17-32. https://doi.org/10.1007/s00190-014-0757-1

Litwiniszyn J. (1974). Stochastic methods in mechanics of granular bodies. *Stochastic Methods in Mechanics of Granular Bodies*, pp. 5-9. https://doi.org/10.1007/978-3-7091-2836-7_1

Manconi A., Casu F., Ardizzone F., Bonano M., Cardinali M., Luca D. C., Gueguen E., Marchesini I., Parise M., Vennari C., Lanari R., Guzzetti F. (2014). Brief communication: Rapid mapping of landslide events: The 3 December 2013 Montescaglioso landslide, Italy. *Nat Hazard Earth Sys.*, Vol. 14, No. 7, pp. 1835-1841. https://doi.org/10.5194/nhess-14-1835-2014

Massonnet D., Rossi M., Carmona C., Adragna F., Peltzer G., Feigl K., Rabaute T. (1993). The displacement field of the Landers earthquake mapped by radar interferometry. *Nature*, Vol. 364, No. 6433, pp. 138-142. https://doi.org/10.1038/364138a0

Song J. J., Han C. J., Li P., Zhang J. W., Liu D. Y., Jiang M. D., Zheng L., Zhang J. K., Song J. Y. (2012). Quantitative prediction of mining subsidence and its impact on the environment. *International Journal of Mining Science and Technology*, Vol. 22, No. 1, pp. 69-73. https://doi.org/10.1016/j.ijmst.2011.07.008

Strozzi T., Luckman A., Murray T., Wegmuller U., Werner C. L. (2002). Glacier motion estimation using SAR offset-tracking procedures. *IEEE Trans Geosci Remote Sens*, Vol. 40, No. 11, pp. 2384-2391. http://dx.doi.org/10.1109/TGRS.2002.805079

Wang J., Peng X. G., Xu C. H. (2011). Coal mining GPS subsidence monitoring technology and its application. *Mining Science and Technology (China)*, Vol. 21, No. 4, pp. 463-467. https://doi.org/10.1016/j.mstc.2011.06.001

Wang X. F., Wang Y. J., Huang T. (2008). Extracting mining subsidence land from remote sensing images based on domain knowledge. *Journal of China University of Mining and Technology*, Vol. 18, No. 2, pp. 168-171. https://doi.org/10.1016/S1006-1266(08)60036-X

Yang C., Zhang Q., Zhao C. (2010). Monitoring mine collapse by D-InSAR. *Mining Science and Technology*, Vol. 20, No. 5, pp. 696-700. https://doi.org/10.1016/S1674-5264(09)60265-9

Zhao C., Lu Z., Zhang Q. (2013). Time-series deformation monitoring over mining regions with SAR intensity-based offset measurements. *Remote Sensing Letters*, Vol. 4, No. 5, pp. 436-445. https://doi.org/10.1080/2150704X.2012.746482

Zhao C., Lu Z., Zhang Q. (2014). Mining collapse monitoring with SAR imagery data: A case study of Datong mine, China. *Journal of Applied Remote Sensing*, Vol. 8, No. 1, pp. 083574-083574, 2014. https://doi.org/10.1117/1.JRS.8.083574